Influence of Phase Transformation on Stress Evolution during Growth of Metal Thin Films on Silicon

A. Fillon, G. Abadias,* A. Michel, C. Jaouen, and P. Villechaise

Institut P', CNRS-Université de Poitiers-ENSMA, Département Physique et Mécanique des Matériaux, SP2MI–Téléport 2, F86962 Futuroscope-Chasseneuil cedex, France

(Received 26 October 2009; published 2 March 2010)

In situ stress measurements during two-dimensional growth of low mobility metal films on amorphous Si were used to demonstrate the impact of interface reactivity and phase transformation on stress evolution. Using $Mo_{1-x}Si_x$ films as examples, the results show that the tensile stress rise, which develops after the film has become crystalline, is correlated with an increase in lateral grain size. The origin of the tensile stress is attributed to the volume change resulting from the alloy crystallization, which occurs at a concentration-dependent critical thickness.

DOI: 10.1103/PhysRevLett.104.096101 PACS numbers: 68.55.−a, 68.35.Gy, 81.15.−z, 81.30.Hd

The use of real-time measurements of stress evolution during the growth of polycrystalline films [1–6] or epitaxial monolayers [7–11] has been shown to offer a sensitive tool to identify different growth regimes with submonolayer sensitivity and has shed some light on the origin of stress generation and relaxation mechanisms. During the Volmer-Weber growth of high-mobility metals, surface stress and grain boundaries [12–14] have been shown to play a decisive role in complex film stress evolution, as well as all surface defects that result from the dynamical growth process [2–5]. Interfacial effects, however, manifest more critically when a layer-by-layer growth mode takes place, as in heteroepitaxy or when a strong chemical affinity exists between film and substrate. In addition to coherency strain [7,8], other mechanisms such as charge transfer [9] or segregation [10,11] have been evidenced as prominent sources of stress change. The minimization of the interfacial energy also promotes the stabilization of nonequilibrium phases, either in the crystalline [15] or amorphous [16] state. However, the influence of this phenomenon on the film stress evolution, as well as the stress change associated with phase transitions, remain largely unexplored. This is an important issue as metastable phases can form during growth of metallic films on suitable substrates.

The observation of distinct stress evolutions in amorphous and crystalline states was first reported in the pioneering studies of Buckel on quenched Ga and Bi films [17]. However, the relation with the change in film density at the amorphous-crystalline transition was not clearly established and no attention was paid on the impact of the nucleation and growth mechanism on the induced-crystalline microstructure of these films. In this Letter, we show that the volume change during the crystallization of interface-stabilized amorphous layers can lead to the development of large tensile stress and large grain sizes. Examples will be given for the case of transition metal-silicon systems, the archetype of these being Mo/Si, which are characterized by a high chemical reactivity at the interfaces and a low atomic mobility of the metal, but for which there is little knowledge on their interplay with stress buildup [18].

Mo/Si multilayers are representative of polycrystalline/amorphous interfaces. However, Mo crystallizes at a layer thickness of ~2 nm [19–21]. We will show that by using $Mo_{1-x}Si_x$ alloys, it is possible to extend the range of thickness under which the amorphous phase can be stabilized. The $Mo_{1-x}Si_x$ films ($0 \leq x \leq 0.5$) were grown at room temperature by magnetron cosputtering under Ar discharge in a high-vacuum chamber (base pressure of $\sim 2 \times 10^{-6}$ Pa). The atomic fraction of Si (x) was varied by changing the respective Mo and Si target powers, and quantified *ex situ* using energy dispersive x-ray spectroscopy with a precision of ~0.5 at. %. Prior to film deposition, ~10 nm amorphous Si (*a*-Si) buffer layer was sputter deposited on oxidized (100) Si substrates at the same Ar working pressure of 0.24 Pa. At this pressure, the mean free path of the particles is less than the target-to-substrate distance (18 cm); thus, the ballistic effect can be neglected. Particular attention was also paid to keep a constant growth rate of $\sim 0.12 \pm 0.01$ nm/s. Hence, the contribution of kinetics on the stress evolution [4,5], if any, would be the same for all films. Immediately after growth, the surface morphology was imaged by atomic force microscopy (AFM) operating in the tapping mode, while crystallographic orientation and grain size distribution were determined by combining x-ray diffraction (XRD) and electron backscattering diffraction (EBSD). The stress evolution in the film was monitored in real time during growth using a multibeam optical stress sensor technique (kSA MOSS) based on the measurement of the substrate curvature. The curvature resolution was 2×10^{-4} m^{-1}, which translates into a sensitivity of 0.09 N/m for 100 μm thick Si wafers. The force in the film per unit width (F/w) is calculated from the measured curvature using the well-known Stoney equation. In a graph of F/w vs film thickness h, the

incremental stress is obtained from the slope $d(F/w)/dh$ and combines the effect of adding a new layer to the film with any stress evolution occurring in the already-grown film.

The stress evolution in various $Mo_{1-x}Si_x$ alloys is shown in Fig. 1(a) over a thickness range of 120 nm. Three distinct types of behavior can be distinguished as a function of the Si content. (i) For $x < 0.15$, a tensile stress is developing after 3–5 nm, which gradually levels off with increasing film thickness and Si content [Fig. 1(a)]. The incremental stress does not exceed ~2 GPa and a slope change of the F/w curves from tensile to compressive is observed at relatively large film thickness ($h \sim 100$ nm). (ii) For $0.16 \leq x < 0.19$, a larger tensile stress of ~3 GPa is developing after 13–20 nm and is maintained at a large film thickness. (iii) For $x \geq 0.19$, the stress becomes rapidly (after 3 nm) compressive with a steady state value of ~ -0.4 GPa and almost independent on the Si content over the range 0.19–0.5. The insets of Fig. 1(b) show that there are minor curvature changes upon growth interruption, both in the compressive and tensile stress states, in marked departure with behaviors observed previously for high-mobility metals [2–4].

XRD patterns [inset of Fig. 1(a)] show that films with $x \geq 0.19$ correspond to metastable amorphous alloys, while for $x < 0.19$, metastable crystalline $Mo_{1-x}Si_x$ solid solutions with a bcc structure and a (110) texture are formed. Therefore, $x = 0.19$ corresponds to the critical Si content (denoted as x_c in what follows) for the crystalline-to-amorphous phase transformation in the bulk state. Note that a phase separation would be expected at equilibrium in the Mo-Si system. Since all depositions occurred at constant deposition rate and working pressure, the observed variations of Fig. 1 cannot be ascribed to kinetic or energetic effects but rather to microstructural changes associated with phase transformation, as described in Figs. 2 and 3.

A closer look at the F/w curves below $h \sim 15$ nm (Fig. 2) provides useful information on the phase transformation and stress change taking place during the early growth stages. Stage I ($h < 0.8$ nm) is characterized by an abrupt tensile rise, due to the surface stress change during the deposition of a Mo-rich film onto Si, and attests of a 2D growth mode. In stage II, an almost constant force plateau is reached and is associated with an amorphous layer formation [see Fig. 3(e)]. This is followed by a transient, but reproducibly observable, stress change at a critical thickness h_c. For pure Mo film, the value of h_c is found to be ~2.2 nm, in good agreement with the reported values of the thickness at which crystallization takes place [19,20]. With increasing Si content, the value of h_c is found to increase significantly, reaching ~27 nm for $x = 0.18$. Postgrowth XRD analysis and transmission electron microscopy observations confirmed that below h_c films were amorphous, while above h_c, transformation of the initially amorphous layer into a bcc crystalline material took place almost down to the Si interface. Note in Fig. 3(e) the presence of an interfacial amorphous alloy with a thickness of ~1.8 nm, also observed in Mo/Si multilayers [21]. Finally, stage III is characterized by the subsequent buildup of tensile stress after h_c, whose amplitude is strongly dependent on the Si content (Fig. 1).

The surface topography of crystalline alloys observed by AFM [Figs. 3(a)–3(c)] shows that the in-plane grain size increases drastically with increasing Si content: for $x = 0.16$ and 0.18, unusually large grains, with a diameter up to

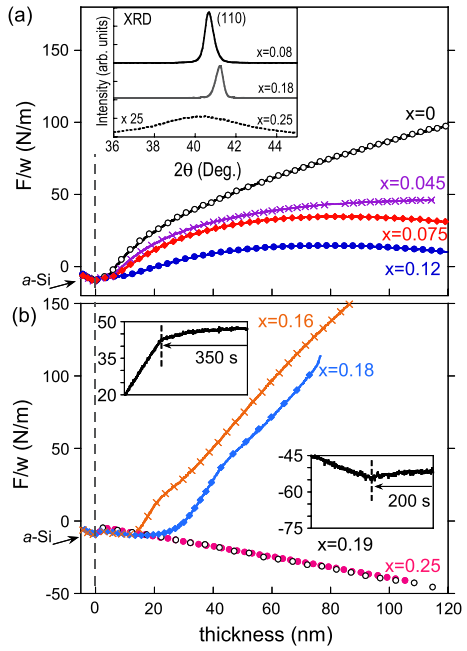

FIG. 1 (color online). Force per unit width during growth of $Mo_{1-x}Si_x$ films on a-Si. (a) $x = 0$, 0.045, 0.075, and 0.12. (b) $x = 0.16$, 0.19, and 0.25. The data for $h < 0$ correspond to the end of the a-Si buffer layer growth. The inset in (a) shows representative $\theta - 2\theta$ XRD patterns of selected $Mo_{1-x}Si_x$ alloys. The insets in (b) show stress evolution vs time after shutter has been closed for $x = 0.16$ and $x = 0.19$.

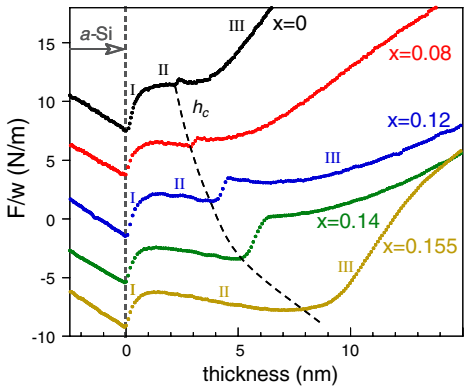

FIG. 2 (color online). Evolution of the force per unit width during the early growth stages of $Mo_{1-x}Si_x$ films with varying x. The dashed line indicates the evolution of the critical thickness h_c for crystallization. Curves have been shifted for the sake of clarity.

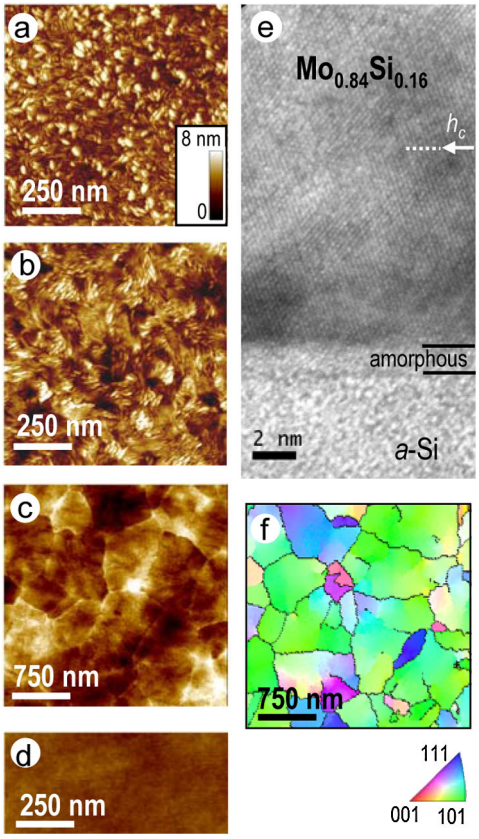

FIG. 3 (color online). (a)–(d) AFM images of ~150 nm thick $Mo_{1-x}Si_x$ films grown on *a*-Si. (a) $x = 0$, (b) $x = 0.08$, (c) $x = 0.16$, and (d) $x = 0.25$. (e) Cross-sectional high resolution transmission electron microscopy image of the $Mo_{0.84}Si_{0.16}$ film deposited on *a*-Si. The value of $h_c \sim 10$ nm is shown. (f) EBSD image of the $Mo_{0.83}Si_{0.17}$ film.

1–2 μm, are formed. EBSD experiments confirm the large-grain microstructure of the $x = 0.17$ [Fig. 3(f)] and 0.18 alloys, with a majority of (110) textured grains. Moreover, analysis of the XRD line broadening shows that the coherence length of the diffracting domains along the growth direction is limited by the film thickness for all crystalline alloys. Thus, the crystalline growth is characteristic of a grain-by-grain epitaxial growth. On the other hand, the amorphous alloys exhibit a featureless surface with reduced roughness [Fig. 3(d)].

Two mechanisms can be invoked to explain the stabilization of metastable amorphous alloy films below h_c. The first one is related to segregation effects which could account for a Si enriched concentration at the free surface due to the surfactant character of Si atoms [22]. Then, the crystallization would occur at a thickness corresponding to a Si concentration lower than x_c [20,21], which is in contradiction with the observation of the almost complete backwards crystallization [Fig. 3(e)]. The second consists in the stabilization at low film thickness of the amorphous phase by minimization of the surface and/or interface energy, despite the chemical driving force towards crystallization. Using the fact that nucleation originates from the surface, we will consider, as proposed by Herr *et al.* [16], an initial disk-shaped crystalline nucleus (radius r, thickness h) inside an amorphous layer of thickness h (see the inset of Fig. 4). In this framework, the Gibbs energy change $\Delta G_{a\text{-}c}(x)$ during the *a*-*c* phase transformation of the $Mo_{1-x}Si_x$ nucleus can be expressed as

$$\Delta G_{a\text{-}c}(x) = \Delta g_{a\text{-}c}(x)\pi r^2 h + \pi r^2[\Delta\gamma_{a\text{-}c}(x) + \Delta\gamma^{\text{int}}_{a\text{-}c}(x)] + 2\pi r h \gamma^{\text{lat}}_{a\text{-}c}(x), \quad (1)$$

where $\Delta g_{a\text{-}c}(x)$ is the Gibbs energy for crystallization per unit volume [$\Delta g_{a\text{-}c}(x) \leq 0$ for $x \leq x_c$], $\Delta\gamma_{a\text{-}c}(x)$ [respectively $\Delta\gamma^{\text{int}}_{a\text{-}c}(x)$] is the difference in surface energy (respectively interface energy with the *a*-Si underlayer) between the amorphous and crystalline phase, and $\gamma^{\text{lat}}_{a\text{-}c}(x)$ is the lateral interface energy between the crystalline nucleus and the amorphous phase. Assuming a regular solution model for the metastable $Mo_{1-x}Si_x$ alloys, $\Delta g_{a\text{-}c}(x)$ can be written as $\Delta g_{a\text{-}c}(x) = \Delta g^0_{a\text{-}c} + \Lambda x(1-x)$, where Λ is the change in chemical interaction parameter ($\Lambda > 0$). For pure Mo, we used the value of $\Delta G^0_{a\text{-}c} = \Delta g^0_{a\text{-}c} V^{\text{Mo}}_{\text{mol}} \approx -30$ kJ mol^{-1} [22]. Increasing the Si content will decrease the driving force towards crystallization. For a given film thickness h, if the term

$$\Delta g_{a\text{-}c}(x)h + \Delta\gamma_{a\text{-}c}(x) + \Delta\gamma^{\text{int}}_{a\text{-}c}(x) < 0 \quad (2)$$

then the complete transformation of an amorphous phase into a crystalline phase by a nucleation and growth mechanism is possible. The condition for the fulfilment of Eq. (2) can be expressed by the critical thickness h_c, as

$$\frac{1}{h_c} = \frac{-\Delta g^0_{a\text{-}c}}{(\Delta\gamma^0_{a\text{-}c} + \Delta\gamma^{\text{int},0}_{a\text{-}c})(1-\alpha x)}\left[1 + \frac{\Lambda}{\Delta g^0_{a\text{-}c}}x(1-x)\right], \quad (3)$$

which is obtained by assuming, in a first approximation, the same linear concentration dependence (coefficient α) of the $\Delta\gamma_{a\text{-}c}$ and $\Delta\gamma^{\text{int}}_{a\text{-}c}$ quantities.

Once the critical thickness is exceed, there exists a critical nucleus radius r_c and an energy barrier W^* for the transformation, r_c and W^* increasing drastically when x reaches x_c. As a consequence, the nucleation rate $J \propto \exp(-W^*/kT)$ decreases with x.

Figure 4 shows the evolution with x of $1/h_c$ determined from the *in situ* stress study. One can see that the proposed model reproduces fairly well the experimental variations of h_c, clearly supporting the balance contribution between the stabilizing interface energy and the volume driving force for crystallization at the critical thickness. When $x \sim x_c$ then h_c diverges and the film remains amorphous at any thickness, as observed experimentally. The relative large value of 5.0 J/m^2 obtained for the sum $(\Delta\gamma^0_{a\text{-}c} + \Delta\gamma^{\text{int},0}_{a\text{-}c})$ is probably overestimated as the value of $\Delta g^0_{a\text{-}c}$ was estimated by taking reference to a perfect Mo crystal. However, the reduction by ~40% obtained for $x \sim x_c$ seems plausible if one considers the large change in chemical free energy with x. The inset of Fig. 4 shows the

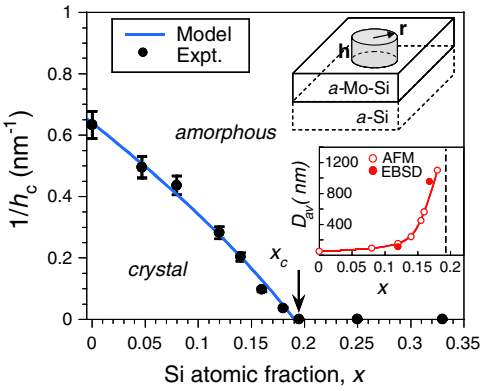

FIG. 4 (color online). Evolution of $1/h_c$ vs atomic fraction of Si (x). The solid line corresponds to the best fit of the thermodynamic model [Eq. (3)] to the experimental data, which is obtained for $\Lambda \sim 194$ kJ $\cdot$ mol^{-1}, $(\Delta\gamma^0_{a\text{-}c} + \Delta\gamma^{\text{int},0}_{a\text{-}c}) \sim 5.0$ J $\cdot$ m^{-2} and $\alpha = 2.2$. The insets show the geometry used for the nucleation model and the evolution with x of the mean lateral grain diameter D_{av}.

evolution with x of the mean lateral grain diameter D_{av} deduced from AFM and EBSD analysis. A noticeable increase of D_{av} is observed with x, directly related to the decrease of the nucleation rate, which supports the model of the polymorphous transformation described above.

In the present study, the largest tensile stresses ($\sigma \sim 3$ GPa) are observed for the films exhibiting the largest grain sizes. This result may appear surprising at first sight, if we compare to what is usually observed for polycrystalline films: the tensile stress, which is due to attractive forces at the grain boundary, inversely scales with the grain size [13,23]. However, the films considered here are not polycrystalline from the beginning of growth. The stress associated with crystallization should be dominated by the volume change at the a-c transformation. Using the Young modulus value of $E = 260$ GPa, as deduced from picosecond acoustic measurements on the $Mo_{0.84}Si_{0.16}$ film, a Poisson ratio of $\nu = 0.3$, the relative change in volume $\Delta V/V = -3\sigma(1-\nu)/\text{E}$ is found to be $\sim -2.5\%$, which is in reasonable agreement with the densification values reported in most metallic alloys [24]. Note that the development of a steady state tensile regime far beyond h_c (stage III) involves the propagation of the elastic strain as the film thickens during the homoepitaxial growth. This is in agreement with the large vertical coherence length of the grains. For the lower Si contents (films with smaller grain sizes, $x < 0.16$), the magnitude of tensile stress is lower, which could be explained by a partial accommodation of the densification strain at the grain boundary. However, the stress evolution in stage III seems more complex than just a relaxation of the tensile component: a compressive stress source appears to counteract the tensile stress one (see Fig. 1). This reveals the preexisting competition between tensile and compressive stress generation in these films with lower grain sizes. Further investigations should be carried out to discriminate between capillarity effects [1,12] or insertion of extra atoms at grain boundary [2,5] as compressive stress sources.

To summarize, we propose a model which accounts for all the features of the growth of low-mobility metals on amorphous substrates, including the interfacial stabilization of an amorphous layer and the onset of tensile stress generation at the a-c transition. Subsequent development of high tensile stresses in layers with large grain sizes is associated with the strain propagation by a grain by grain epitaxial growth. More generally, this work addresses the issue of the correlation of metal-silicon reactivity and phase transformation to stress development, which is of prime importance for many thin film applications, e.g., in microelectronics or photovoltaics.

*Corresponding author.
gregory.abadias@univ-poitiers.fr

[1] R. Abermann, R. Kramer, and J. Mäser, Thin Solid Films **52**, 215 (1978).
[2] E. Chason *et al.*, Phys. Rev. Lett. **88**, 156103 (2002).
[3] C. Friesen and C. V. Thompson, Phys. Rev. Lett. **89**, 126103 (2002).
[4] A. L. Del Vecchio and F. Spaepen, J. Appl. Phys. **101**, 063518 (2007).
[5] B. W. Sheldon *et al.*, J. Appl. Phys. **98**, 043509 (2005).
[6] G. Abadias and Ph. Guerin, Appl. Phys. Lett. **93**, 111908 (2008).
[7] G. Wedler *et al.*, Phys. Rev. Lett. **93**, 236101 (2004).
[8] R. Mahesh *et al.*, Phys. Rev. B **68**, 045416 (2003).
[9] A. Grossman *et al.*, Phys. Rev. Lett. **77**, 127 (1996).
[10] J. A. Floro and E. Chason, Appl. Phys. Lett. **69**, 3830 (1996).
[11] S. Labat *et al.*, Appl. Phys. Lett. **75**, 914 (1999).
[12] R. C. Cammarata, T. M. Trimble, and D. J. Srolovitz, J. Mater. Res. **15**, 2468 (2000).
[13] W. D. Nix and B. M. Clemens, J. Mater. Res. **14**, 3467 (1999).
[14] F. Spaepen, Acta Mater. **48**, 31 (2000).
[15] T. C. Hufnagel *et al.*, J. Appl. Phys. **85**, 2609 (1999).
[16] U. Herr *et al.*, Phys. Rev. B **59**, 13 719 (1999).
[17] W. Buckel, J. Vac. Sci. Technol. **6**, 606 (1969).
[18] J. M. Freitag and B. M. Clemens, Appl. Phys. Lett. **73**, 43 (1998).
[19] D. G. Stearns *et al.*, J. Appl. Phys. **67**, 2415 (1990).
[20] S. Bajt, D. G. Stearns, and P. A. Kearney, J. Appl. Phys. **90**, 1017 (2001).
[21] C. Largeron, E. Quesnel, and J. Thibault, Philos. Mag. **86**, 2865 (2006).
[22] The surface energy of a-Si (0.827 J $\cdot$ m^{-2}) is much lower than that of (110) bcc Mo ($\sim$3.0 J $\cdot$ m^{-2}), see Q. Liang, H. M. Lu, Surf. Sci. Rep. **63**, 427 (2008).
[23] L. B. Freund and E. Chason, J. Appl. Phys. **89**, 4866 (2001).
[24] P. H. Gaskell, in *Models for the Structure of Amorphous Metals*, edited by H. Bech and H. J. Güntherodt, Glassy Metals Vol. II (Springer Verlag, Berlin, 1983).